Journal of Harbin Engineering University Vol 44 No. 7
ISSN: 1006-7043 July 2023

Influence of Cryo-milling on metal matrix interface and characteristics of AA5154 – ZrC composites

P. Thangavel*, S. Prakasam, K. M. Arunraja, K. Kannakumar

Shree Venkateshwara Hi-Tech Engineering College, Gobichettipalayam, Erode-638455, Tamilnadu.

*Corresponding Author: thangspro@gmail.com

Abstract

This study presents the impact of cryomillingpressure less sintered AA5154-xZrC (x = 6, 12, 18 wt%) composites on their microstructural and mechanical properties. Cryogenic milling of composite powders in the presence of liquid nitrogen yielded dense compacts, which were then pressure-lessly sintered at 650°C for 5hours in an Argon/Hydrogen atmosphere. Cryomillingtime(15 or 30 min) and ZrC content significantly impact the density, elastic modulus, microstructures, and mechanical parameters of the sintered specimen (6, 12, 18 wt%).Bulk samples of AA5154 matrix composites strengthened with 6-18 wt% ZrC particles were obtained after 15 minutes of cryomilling, followed by pressure less sintering; the results showed relative densities between 97.41 and 98.52%, hardness values between 0.78 and 1.42 GPa, wear volume losses between 0.281 and 1.272 mm^3, and elastic moduli between 284.3 and 434.7 GPa.

Keywords: Cryo-milling,ZrC, Aluminum, metal matrix composites, mechanical properties.

1. Introduction

Higher specific modulus and strengths, like wear and creep resistances, have piqued the interest of the aerospace and automotive industries in AA5154-based metal matrix composites (MMCs) enhanced using continuous/discontinuous reinforcements[1]. When a ductile Al-based matrix combines with various high-strength reinforcements, the resulting composites are lightweight and have increased specific strengths [2]. Creating ideal combinations of the matrix, reinforcing material, and manufacturing process is the key to meeting the expanding demand across various industrial applications [3], [4].

Some researchers have observed that intermetallic Al_3Ti formed during the manufacturing of Al-ZrC composites, drastically lowering some mechanical parameters like wear resistance and fatigue life[5],[6]. Therefore, it is of interest to avoid the production of this unfavorable Al_3Ti phase when the powder metallurgical technique is employed[7]. To reduce the likelihood of any adverse interactions occurring between the matrix and reinforcement, mechanical alloying (MA) has been used as a powder preparation process for composites [8]–[10]. Al_3Ti flakes in trace amounts in Al-ZrC composites prepare using MA, followed by sintering procedures [11]. Cryomilling (CM) is a powder preparation method that, like MA, uses high-energy milling in cold conditions like liquid nitrogen [12]. Cryogenic milling allows for shorter milling times, smaller grains, and less particle aggregation due to the minimum temperatures in the cryogenic medium[13], [14].

Additionally, it can prevent unfavorable reactions from occurring while milling and transferring high energy to the powders [15]–[17]. Powder preparation by CM before sintering appears to be a promising technique for AMCs supplemented with ZrC particles[18].

This research suggests a new method for making ZrC particulate-reinforced AMCs, utilizing CM and pressure-less sintering. Interface impacts on CM microstructures in composites analysis. Additionally, the results of the microstructure and mechanical characteristics were studied related to the ZrC content and the CM time.

2. Experimental arrangement

2.1. Processing of specimen

The composite powders merge AA5154 as the matrix and ZrC powders as the reinforcement.

Using a Turbula blender, researchers combined powdered AA5154 and ZrC for 30 minutes to create three different compositions: AA5154-6wt%ZrC, AA5154-12 wt.%ZrC, and AA5154-18 wt%ZrC. For 15 to 30 minutes, the mixes were cryomilled to create the composite powders. Because iron contamination in the samples from the milling medium is inevitable and becomes severe for milling intervals above 30 minutes, the choice of CM times of 15 and 30 minutes appears reasonable. The milling containerfixes in a cryogenic state by circulating liquid nitrogen outside the device. Milling vials were loaded, sealed, and unloaded in a glove box while exposed to Ar gas.

2.2. Sintering

Compaction of each powder mixture at 400 MPa after CM yielded cylindrical shapes with a diameter of 12.8 mm. Like the cylindrical structure, each powder composite compresses to create a standard tensile test sample[19]. High-temperature controlled environment furnace was used to sinter all compacts at 650°C for 5 hours at a heating and cooling rate of 10°C per minute. Since researchers didn't want the compacts' surfaces to oxidize during the sintering process, researchers used an Ar/H2 gas flow atmosphere. Researchers will refer to sintered specimensmade from composite powders synthesized through cryomilling for 15 or 30 minutes as AA5154-ZrC-15 and AA5154-ZrC-30 (x=6, 12, 18), respectively.

2.3. Characterization

A study of composite powders and sintered specimensconduct using X-ray diffraction (XRD) with CuK (= 1.5406) radiation in the 10-90° range on anadvanced Series powder diffractometer at a step size of 0.02° and a rate of 2°/min. The bulk sampleby rolling out cylinders 12.7mm in diameter and 5mm in length. Two models of the sintered sample used a conventional procedure to provide a scratch-free mirror finish; this was necessary before microstructural investigations, indentation measurements, and wear tests[20]. The specimens were ground and polished after being hot-mounted. The bulk samples were scanned with an SEM at 15 kV to get backscattered electron pictures. The Ultra Plus field emission SEM was outfitted with an energy-dispersive X-ray spectrometer (EDX) detector to perform secondary electron SEM imaging and EDX analysis on a subset of the samples. Using the Archimedes method, researchers measured the density of ethanol solutions containing two specimens of each type and reported the average of these data[21].

Tribotester with a 6mm alumina ball sliding at 5mm/s, a 2mm stroke length, and a 3N applied force, covering 25m. A 6M Stylus profilometer employs to analyze optical microscope (OM) screenings of worn surfaces. It reports that the vertical and horizontal tolerances of the sintered samples had changed. To determine each sample's relative wear resistance, researchers divided its maximum wear volume loss by its average wear volume loss[22]. The Ultra Plus field emission SEM was used to take pictures of the wear patterns on some samples[23].

At a peak load of 50 mN, a nano-indenter employs to measure the depth of the samples. Researchers could get load displacement curvatures from the AA5154 matrix and ZrC reinforcements of the sintered specimen without having to hold them at the maximum load for any time. The results of nanoindentation studies on sintered materials, along with the matrix's hardness range, elastic modulus, and strengthening. Vickers microhardness range was evaluated for specimen at 30g for 15s using a hardness tester to assess the degree to which projected hardness of the composites matched the experimented data. The stress-strain curvatures were obtained from tensile strength measurements using a universal tester with a 10kN capacity[24]. Researchers averaged three lessons at each stress-strain curve node for each sample.

3. Results and discussion

Powders of AA5154-6ZrC, AA5154-12ZrC, and AA5154-18ZrC were CM for 15 and 30 minutes, and their XRD patterns indicate in Fig. 1. For both milling times, the intensity of the ZrC peaks increased slightly as the ZrC content moved from 6 to 18 wt percent. The XRD peaks of AA5154 and ZrC phases showed no appreciable widening due to

the increased CM duration (from 15 to 30 min). Particle degradation and the start of intermetallic phase production can occur during milling procedures due to cold welding, fracturing, and rewelding mechanisms [25].

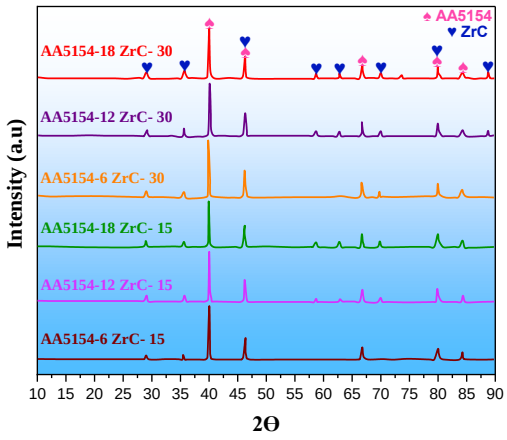

Fig. 1. XRD patterns of different samples (AA5154, ZrC)

In addition, the XRD was used to its full extent (>2 wt percent of the specimen), and no wear-off impurities from the cryo-milling medium discover. But XRF studies showed that Ag contamination did occur, with amounts of 4.5and 6.3 ppm for the AA5154-12ZrC powders cryo-milling time for 15 and 30 minutes, respectively. After further sintering, the Ag impurities in the cryo-milled specimenfor 15 and 30 minutes to minimal. As the Ag impurity content of the AA5154-12ZrC powders increased to 11.5ppm after being subjected to CM for 30 minutes, this supports using the shorter CM intervals as a heuristic tool.

One advantage of the CM method is that it allows grains torefine fasterand, in less duration, than conventional milling. The mean crystallite dimensions of the AA5154phases in the 15 and 30-min cryomilling AA5154-6ZrC, AA5154-12ZrC, and AA5154-18ZrC powders indicate in Table 1. As CM duration increased from 15 to 30 min, there was a drastic reduction (>36%) in the mean crystallite size of the Aluminummedium. After one hour of milling, the average crystallite size of mechanically alloyed AA5154-xZrC (x = 6, 12, and 18 wt %) powders reported around 175nm [25]. This powder has smaller mean crystallite sizes (175 nm) than the mechanically alloyed powder, even after 15 minutes of CM application at cryogenic temperatures. Since ZrC is hard and brittle and the milling occurs in a cryogenic environment, the mean crystallite dimensions decrease as the ZrC portion rises from 6 to 18 wt %.

X-ray diffraction (XRD) patterns of sintered bulk samples of AA5154-6ZrC, AA5154-12ZrC, and AA5154-18ZrC cryomilling for 15 and 30 minutes indicate in Figure2. The sintered product consists entirely of Al and ZrC. (Fig. 2). After 15 minutes of CM, no secondary phases were present; this lends credence to the use of chemically stable ceramic reinforcement particles in light-metal matrix systems. However, XRD profiles for the sintered AA5154-6ZrC, AA5154-12ZrC, and AA5154-18ZrC samples reveal that an Al_2O_3 phase formed after the prolongedcryo-millingduration of 30 min. Compared to the AA5154-18ZrC specimen, the X-ray diffraction peak for the Al_2O_3 phase is less prominent in the AA5154-6ZrC and AA5154-12ZrC samples (Fig. 2). To produce contaminant-free reinforcement and matrix interfaces, more time spent in CM makes more reactive surfaces, leaving the powders vulnerable to any reaction that may occur during handling.

After being CM for 30 minutes and then sintered, AA5154-6ZrC, AA5154-12ZrC, and AA5154-18ZrC samples indicate 0.41, 0.68, and 0.99 wt% O;correspondingly, according to EDX tests. These percentages of oxygen are about equivalent to the ratio of the Al_2O_3 phase in samples of AA5154-6ZrC, AA5154-12ZrC, and AA5154-18ZrC, respectively. Even though Al_2O_3 creates after the sintering, it might serve as a reinforcing agent, increasing the hardness and mechanical characteristics. Specific studies on creatingaluminum metal matrix compositescryomilling in a liquid nitrogen environment have found secondary phases, such as AlN and Al (ON), after sintering [26], [27]. However, in this study, when CM conducts with liquid nitrogen circulating outwardlyabout the milling container, neither nitride- nor oxynitride-based compounds were produced. In addition, the

milling vial/balls showed no signs of Ag impurities after sintering, indicating that the level was 2wt%.

The Al_3Ti phase and other brittle reaction products detect at the reinforcement/matrix interfaces during casting and powder metallurgy manufacture of Al-ZrC composites [28], [29]. Previous studies by author[30] show that the significant increase in impact energy and temperature produced by the persistence of impacts and the partial melting of AA5154 at the sintering temperature weakens the ZrC bonds during mechanical alloying and sintering. Milling at lower temperatures (15 and 30 minutes) and with less energy input (sintering) may explain why the intermetallic phase Al_3Ti did not occur in the samples. Diffusion processes are hindered at cryogenic temperatures, giving CM an advantage over milling at an average temperature [31].

Table 1 Mean crystallite sizes and milling time of individual specimen.

Specimen Name	Mean Crystallite Size	Milling Time
units	**(nm)**	**(min)**
AA5154 – 6ZrC	175	15
AA5154 – 12ZrC	115	15
AA5154– 18ZrC	106	15
AA5154 – 6ZrC	105	30
AA5154 – 12ZrC	75	30
AA5154– 18ZrC	67	30

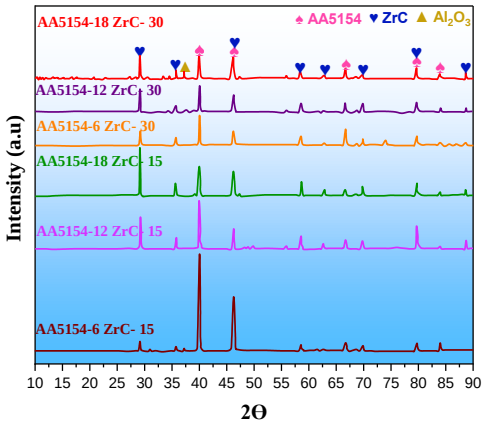

Fig. 2. X-ray Diffraction patterns of the different specimens (AA5154, ZrC, Al_2O_3)

The backscattered electron SEM images in Fig. 3(a)-(f) show bulk samples sintered from AA5154-6ZrC, AA5154-12ZrC, and AA5154-18ZrC powders and CM for 15 and 30 min. ZrC builds up and spreads evenly throughout the microstructure during both CM times. On the other hand, the microstructures of the cryo-milling and sintered specimen did not display the fundamental concerns met in casting techniques, like the lack of adequately dispersed reinforcing particles. ZrC particulate-reinforced Al matrix contain Al_3Ti phases as flake-like structures in previous studies [32], [33]. However, in the SEM pictures shown in Figure 3(a)-(c), no evidence of flake production (f). The specimen's X-ray diffraction analysis (Figure. 2) corroborated the lack of Al_3Ti flakes. Higher porosities were also seen in the sintered samplescryo-milling for 30 minutes compared to 15 minutes, which may be due to trace quantities of the Al_2O_3 phase.

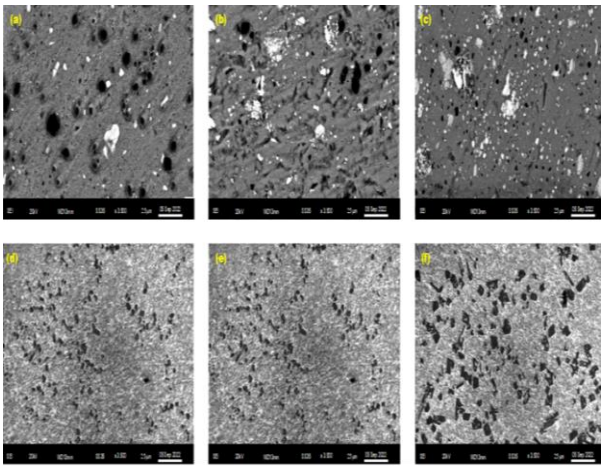

Fig. 3. BESEM pictures of: (a) AA5154-6ZrC-15, (b) AA5154-12ZrC-15, (c) AA5154-18ZrC-15, (d) AA5154-6ZrC-30, (e) AA5154-12ZrC-15, and (f) AA5154-18ZrC-15.

Samples sintered due to CM inhibited the formation of secondary phases in the Aluminum and ZrC contents. The AA5154-6ZrC, AA5154-12ZrC, and AA5154-18ZrC manufactured in this study avoid issues such as forming thick Al_3Ti flakes, the splintering of thin Al_3Ti slivers, the presence of crashes and voids on the outer edges of the Al_3Ti chips, and the decrease in dense rate. SEM images and EDX maps of the matrix/reinforcement interface collects from a specimen of AA5154-12ZrC-15 to examine the uniform transition between the matrix and the reinforcement (Fig. 4). The elemental maps for Ti and B nearly entirely overlap, reflecting the prevalence of ZrC materials.

SEM and EDX studies (points +a, +b, +c) of a sintered AA5154-18ZrC-30 sample show that the matrix indicates the lighter gray particles (Fig. 5). At location +a, EDX readings have confirmed that only aluminum is present. White particles of varied sizes and shapes at the interface between +b and +c. X-ray diffraction (XRD) examination (Fig. 2) and elemental analysis (EDX) at location +b both unambiguously identify Al_2O_3 as the parent component. Ti and B, together with Al (0.56 at. %) from the matrix, were found to be the most abundant elements in the EDX analysis of the particulate strengthen labeled as +c in the scanning electron microscopic picture. Microstructural investigations also confirmed the presence of Al_2O_3 contamination inside the deposited zone of the composite and within the first 30 minutes of the cryo-milled and sintered specimen.

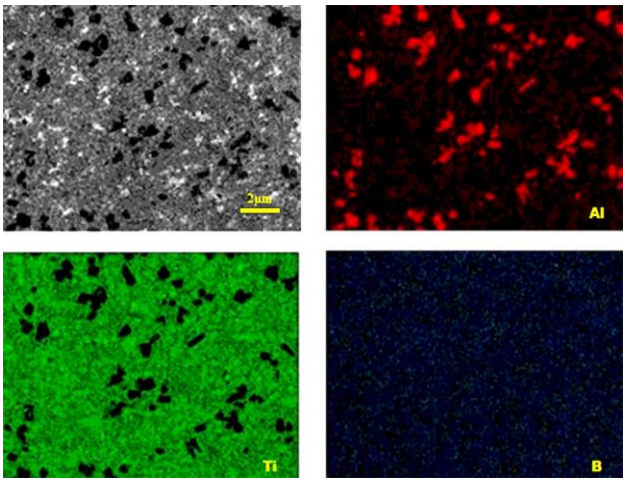

Fig. 4. The matrix-reinforcement interface in the sintered AA5154-12ZrC-15 specimen, as seen in a secondary electron scanning electron microscopic picture and as mapped by EDX.

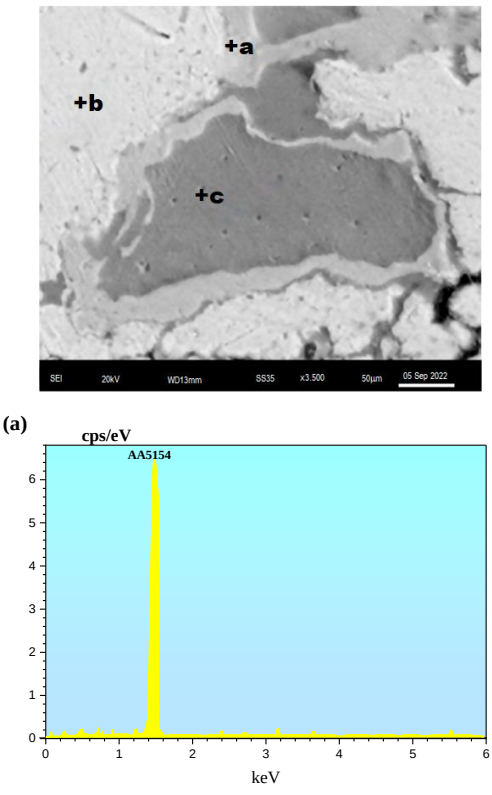

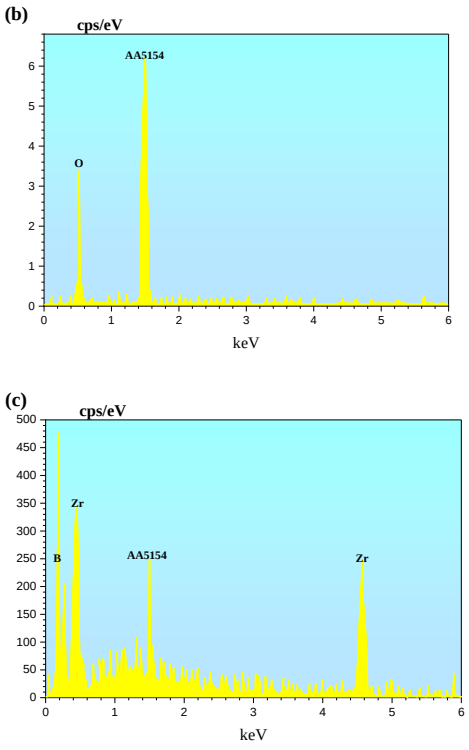

Fig. 5. Sintered AA5154-18ZrC-30 sample secondary electron SEM image and EDX analysis.

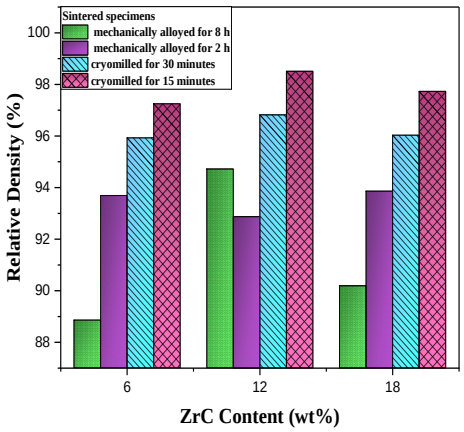

Fig. 6. Relative density of the specimen

Fig.6 displays bulk samples sintered from AA5154-6ZrC, AA5154-12ZrC, and AA5154-18ZrC powders cryo-milling for 15 and 30 min.) along their unique density-ZrC content curves. Furthermore, Fig 6. shows specimens sintered from mechanically alloyed (MA'd) powdersfor a density scale to help visualize differences (adapted from [34]). Compared to AA5154-6ZrC and AA5154-18ZrC, the relative density values (98.52 and 97.41%) of AA5154-12ZrC samples are greater (both 15 and 30 minutes of CM). Additionally, AA5154-12ZrC (Figure. 6) had the density value (94.72%) among AA5154xZrC (x = 6, 12, and 18 wt%) specimenmechanically alloyed for 8 h and sintered [35]. It indicates that adding ZrC to the Al matrix only increases the density to a certain point.

By moving from MA milling to CM milling before sintering, researchers were able to achieve a higher degree of densification at the same ZrC content (12 wt%) (Fig. 6), although this improvement was contingent on the effectiveness of particle size lessening without releasing impurities. Cryo-milling yielded a higher density than mechanical alloy for any given concentration of ZrC. Compared to samples that were CM'd for 30 minutes, all samples that were cryo-milling for 15 minutes exhibited higher relative density values. Crystallite sizes reduce after 30 minutes of CM time, but no further densification attain via sintering. Sintering the 30-minutecryo-milling powders resulted in the formation of an Al_2O_3 phase (Figures. 2), which explainsthe porous structures in the sintered composites (Figs. 3(d)-(f)). Sintering could not successfully bond the ZrC reinforcement and the inevitable byproduct Al2O3 with the Aluminium matrix due to the significant number of defects introduced by cryo-milling. The densification rate of the composites lessens due to the unanticipated Al_2O_3 production.

The wear profiles, shown in Fig. 1, illustrate the changes over time in the sintered specimen's infiltration depth and horizontal detachment. Regarding vertical and horizontal distance, the AA5154-6ZrC-15 sample was superior to the others. When the ZrC content increased from 6 to 12 wt%, the penetration depth and horizontal distance significantly reduced, while the CM duration remained unchanged at 15 minutes. The penetration deepness and flatlengthlessen with an increase of ZrC from 12 to 18 wt%. The change from 6% to 12% wt was more dramatic than the others. Increasing the CM time had a noticeable impact on the AA5154-6ZrC samples, as evidenced

by the fact that the AA5154-6ZrC-30 sample had noticeably less depth and distance than the AA5154-6ZrC-15 specimen. The primary reason for this outcome is the decrease in average crystallite size coupled with the increase in particle surface area. That is to say, as CM times grew longer, a more significant percentage of particle surfaces were able to withstand stresses and friction.

The creation of the stiff and resilient Al_2O_3 phase may be responsible for the reduced wear properties, uniform though just 6wt% ZrC was used to reinforce the Al matrix. The AA5154-18ZrC-30 sample had minorpenetration depth and horizontal distance standard deviations. During wear tests, the ball's ability to slide may be hindered by the formation of Al_2O_3, especially at the matrix/reinforcement contacts. A higher percentage of ZrC in stir cast and forged AMCs increases their resistance to corrosion and wear [36]. Scientists found that aluminum oxide coatings formed at the sample surfaces, preventing the underlying fractures from furtherdecline[37]. These coatings mainly formed due to the microstructure and distribution of ZrC within the tent. Because the Al_2O_3 phase appears in the microstructure as anintermittent layer, it is not surprising that wear resistance improves with increasing ZrC content.

Table 2 displays the sintered samples' wear volume losses and wear resistances. Wear resistance was lowest, and wear loss was greatest (1.272 mm^3) in the AA5154-6ZrC-15 sample (only 1.00). By dividing the volume of wear experienced by the sample by the volume of wear experienced by the composite, the relative wear resistance of this AA5154-6ZrC-15 sample determine. As shown in Fig. 1, the variable penetration deepness and horizontal detachmentare consistent with a rise in ZrC content at a constant CM duration or an increase in cryo-millingduration at a ZrC content leading to improved relative wear resistance. Compared to the AA5154-6ZrC-15 (wear resistance = 1.2), the AA5154-6ZrC-30 (wear resistance = 3.31) shows a dramatic drop in relative wear resistance. When comparing the wear resistance of the AA5154-12ZrC-15 (resistance 3.62) and the AA5154-12ZrC-30 (resistance 3.92), there was little to no discernible change. The resistance gap between the 15-minute CM'd, and sintered samples (resistance 4.61) and the 30-minute samples (resistance 4.69) shrank even further when the ZrC content climbed to 18 wt%. Accordingly, AA5154-12ZrC and AA5154-18ZrC don't differ greatly in their wear resistance over a long period of CM time. In contrast, the AA5154-18ZrC-30 sample demonstrated the greatest wear resistance among the whole set.

There was no noticeable variation in relative wear resistance between specimens sintered from powders CM'd for 30 min, and those CM'd for 60 min due to the contribution of the Al_2O_3 phase to the sliding wear mechanism. Hardness, strength, and wear resistance of the composites with increasing volume fraction of Al_2O_3 up to 10 vol % in a recent work that looked at the impact of Al_2O_3 particles on AMCs made by magnetic milling and hot pressing [38]. Another study by author [39]described the strong wear resistance of AMCs due to Al_2O_3 reinforcing particles as abrasion resistance and deformation restriction. Similarly, AMCs with Al_2O_3 reinforcement (up to 2 wt%) manufactured using liquid metallurgy combined with PM reports have significantly enhanced mechanical characteristics [40]. The wear resistance value of the AA5154-18ZrC-30 sample is greater than that of the other specimens due to the incorporation of 18 wt% ZrC and the subsequent production of Al_2O_3.

Table 2 Wear properties

Specimen	**Wear Volume Loss**	**Relative Wear Resistance**
units	**(mm^3)**	**(%)**
AA5154 – 6ZrC – 15	1.272	1.2
AA5154 – 12ZrC – 15	0.362	3.62

AA5154 – 18ZrC – 15	0.281	4.61
AA5154 – 6ZrC – 30	0.392	3.31
AA5154– 12ZrC – 30	0.328	3.92
AA5154– 18ZrC – 30	0.276	4.69

Figs. 2 of the supplemental data show SEM images of wear fracture acquired from AA5154 – 6ZrC and AA5154-18ZrC specimens sintered from the 15-min cryo-milled powders. The wear track on the AA5154-6ZrC sample was more extensive, as seen in Fig. 2, which shows deep, continuous grooves successivelysimilar to the glidingpath. The AA5154-18ZrC specimen showed a flatter surface, a thinner wear track, andseveral ruptured areas.

The wear resistance value was lowest for AA5154-6ZrC sintered from 4h MA powders and highest for AA5154-18ZrC [41]. Based on the findings of this research, a higher concentration of ZrC particles infused into the matrix acts as an impediment to the movement of dislocations, slows the flow of the material, and increases the resistance to plastic deformation, all of which serve to prevent plastic deformation during sliding under applied loads. Recrystallization and grain growth are hampered by reinforcing particles and some impurities, according to several studies [42]. In addition, the strong wear resistance values observed in AA5154-18ZrC samples were primarily attributable to the lack of Al_3Ti in composites due to the rigidity of the ZrC particles introduced by CM before sintering [43].

Nanoindentation measurements reveal the composites' particle reinforcement, mechanical matrix properties, and matrix wear characteristics. To illustrate, here are some figures—load-displacement curvatures for the sintered specimenAA5154 matrix and ZrC reinforcement in Figures 7 and 8. The low density of the ZrC reinforcement in the AA5154-6ZrC-30 sample prevented any indentation tests from being performed on it (95.82%). The highest penetration depth in the matrix for AA5154-6ZrC-30 and AA5154-18ZrC-30 samples was approximately 1862nm and 1527nm at the 50mN maximal force shown in Figure. 7. For comparison, Fig. 8 displays the maximum and minimum penetration depths in the fortified for the AA5154-12ZrC-30 and AA5154-18ZrC-15 specimens to be roughly 367 and 306nm, respectively. Figure 8 shows that when the ZrC concentration in the composites increases from 12 to 18 wt%, the curves of the sintered samples move to lower indentation depths, confirming the favorable effect of ZrC particles seen for the wear resistances. Indentation of the Al matrix revealed significantly more plastic deformation dissipation than the ZrC reinforcements (Fig. 7), as predicted (Fig. 8).

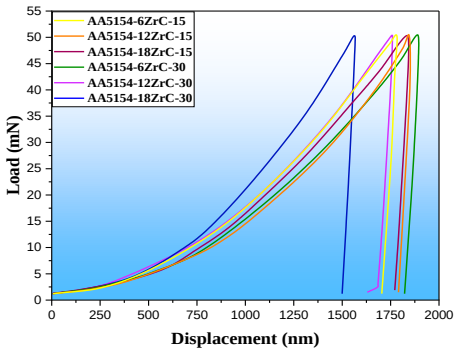

Fig. 7. Load-displacement curvatures for the AA5154 matrix.

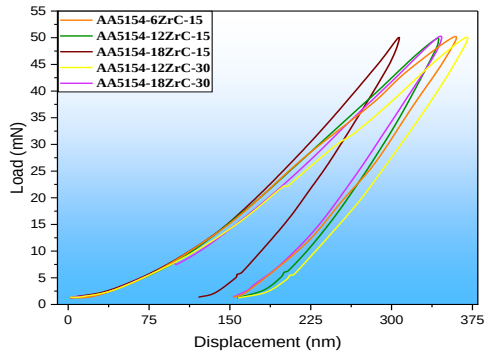

Fig. 8. Load-displacement curvatures for the ZrC reinforcement.

Table 3 displays the Oliver - Pharr method-obtained hardness and elastic modulus range for the composite components. When using 18 wt % ZrC and CM durations of 15 and 30 min, the matrix, reinforcement hardness, and flexible modulus values were the highest (Table 3). The ZrC reinforcement's hardness reduced from 44.71GPa to 34.89GPa, and its elastic modulus decreased from 434.7 GPa to 325.8GPa when the CM time increased from 15 to 30 minutes, although maintaining the same 18 wt percent ZrC content. However, as CM duration from 15 min to 30 min, the Al matrix's elastic modulus rose from 110.4 GPa to 144.8GPa, andthe hardness increased from 0.65 GPa to 0.91GPa.

These findings make sense in light of Fig. 5's microstructural characterization, which reveals evidence of Al_2O_3 production in the matrix/strengthening interfaces, causing a decrease in ZrC strengthening (Table 3). Densification rates of composites reduced as CM time increased because ZrC reinforcement degraded and suffered changes in hardness and elastic modulus values (Figure. 6). The solidification of the stiff and sporadic ZrC particles was significantly affected by the densification of the composites. In contrast, the mechanical energy given by CM was critical in strengthening the ductile main aluminium alloy matrix. On the other hand, no correlation was found between composite density (Fig. 6) and reinforcing hardness (ZrC content), suggesting that these two properties are not directly related (Table 3).

Table 3 Mechanical properties of the specimen

Specimen	**Hardness**	**Elastic Modulus**
units	(**GPa**)	(**GPa**)
AA5154-6ZrC – 15	0.65	107.2
AA5154-12ZrC – 15	0.71	108.6
AA5154-18ZrC – 15	0.65	110.8
AA5154-6ZrC – 30	0.63	110.2
AA5154-12ZrC –30	0.72	102.1
AA5154-18ZrC – 30	0.91	144.3

In addition, the clean interface with the absence of secondary phases, which substantially reach during cryo-milling for 15 minutes, is responsible for the hardness (GPa) and elastic modulus (GPa) of ZrC in the AA5154-18ZrC-15 sample. Nanoindentation testing evaluates the elastic modulus of aluminium alloy, with reported values as low as 69 GPa [44]. None of the data shown in Table 3 of the current investigation come close to this value. Table 1 shows that after 30 minutes of CM, the Al phase (with a crystallite size of 66nm) in the composite powders was refined, significantly increasing the final composites' matrix strength. Therefore, the AA5154 matrix grain size reduction to a strengthening mechanism in ZrC particulate-reinforced aluminium alloy matrix composites [45]. One can calculate the composites' hardness with equation (1). (Assuming isotropic materials).

$$H_c = H_m f_m + H_r f_r \quad (1)$$

where the composite hardness H-c, matrix hardness Hm, reinforcement hardness Hr, and the matrix fraction fm and reinforcement fraction fr. The hardness range from Eqn (1) equated with experimented data for the 15-minute cryo-milled and sintered specimen to test the instruction of composites. Typical Vickers microhardness readings and computed hardness range for the chosen sintered sample (Table 4). The AA5154-6ZrC-15 compressed to a pressure of 0.78, 1.25, and 1.42GPa. Nanoindentation testing on a specimen ofAl-15,TiB_2.Revealed hardness values of 0.64 for Al and 43.62GPa for,TiB_2. Using the values forHm andHr from Table 3, the composite's hardness is 1.51GPa using equation (1). TheHc. values for the AA5154-6ZrC-15 and AA5154-12ZrC-15 composites are estimated to be 0.85 and

1.42GPa, respectively. Table 4 summarizes the computed hardness values, which correlate well with the experimental results, providing more evidence for the model's reliability. As there is no transitional state between the matrix and the reinforcement, it is possible to perform the calculations. Furthermore, the composites' hardness range waspointedly higher than those of monolithic Al and other AMCs strengthened with other particles in experiments and theoretical calculations [46].

Table 4 Comparison of experimented and theoretically Predicted Hardness values.

Specimen Name	Experimented hardness (GPa)	Theoretically Predicted Hardness (GPa)
AA5154 – 6ZrC – 15	0.78± 0.11	0.85
AA5154 – 12ZrC – 30	1.25± 0.17	1.36
AA5154 – 18ZrC – 30	1.42± 0.20	1.51

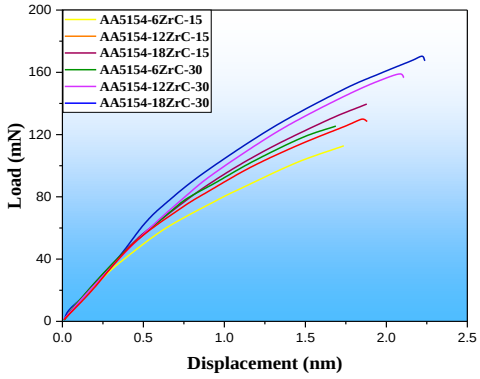

Fig. 9. Stress-strain curvature of the specimen.

Stress-strain curves typical of sintered materials attained during tensile testing (shown in Figure. 9). The stress-strain curvatures for the AA5154-18ZrC-30 composite initiate to depart from the linear elastic area at a stress of minimal 60MPa, as can be shown in Figure 9. The tensile stress risesuninterruptedly to 186MPa. Due to the specimen fracture before attaining the maximum pressure for a perfectly dense specimen, this Figure represents the fracture strength [47]. Every composite exhibits the same behavior. It shows that the sintering requirements for the tensile model were not reached during production using the cold pressing and pressure-less sintering technique. A hot extrusion process has previously manufactured the coarse-grained portions of AA5154-ZrC tensile specimens to accomplish elongation in the plastic deformation direction [48].

The end product of these procedures is a material with exceptional strength and extraordinary plasticity [49]. But the accumulative roll bonded AA5154-ZrC composites [50]had a maximum tensile strength of about 172MPa with low elongation (up to 0.4 %). In addition, the ultimate tensile strength and elongation of Al-7Si/10ZrC composites produced through the salt reaction method were respectively determined to be 210 MPa and 4.6%[51]. Figure 9 shows that fracture strengths did rise with increasing ZrC concentration, as predicted by the investigations above.

Wear resistance, microstructure, interface, density, hardness range, and mechanical properties of the final products were all improved full content of ZrC particles (18 wt%) and short cryo-milling (15 minutes) as a powder technique preceding pressure-less sintering. The mean crystallite size of the Aluminum phase reduced, dense increased, penetration deepness changes reduced, and the composites showed higher relative wear resistance values when the amount of ZrC particle reinforcement was raised (up to 12 wt%).

Using the cryo-milling technique, the microstructure and mechanical properties of composites by the growth of rigid and fragile ZrC in the Aluminium matrix. Long-term and real-world performance studies are needed before ZrC particulate-reinforced AMCs developed in this work may be employed in structural engineering components in the aviation, army, and motorized

industries. Because of its simplicity and benefits, i.e., shorter milling durations and lack of undesirable intermetallic phases, this technology will encourage further research into producing metal particulate-strengthened aluminum metal matrix composites.

4. Conclusions

This investigation seeks to ascertain if cryomilling AA5154-xZrC (x = 6, 12, or 18 wt%) changed its microstructure and mechanical qualities. Following are some inferences from the data:

- All the powders produced by the cryomilling process were made solely of AA5154 and ZrC, with no other materials present. The mean crystallite size of the powders was decreased more by cryo-milling for 30 minutes than by 15 minutes. Cryo-milled samples for 30 minutes, but not 15 minutes, showed Al_2O_3 secondary phase development in the matrix/reinforcement interface after sintering. Milling at cryogenic settings precluded the development of Al_3Ti, typically detected at the boundaries of the sintered AA5154-ZrC composites, uniform at concentrations of up to 18wt% of ZrC. Microstructural analysis revealed that ZrC dispersed throughout the AA5154 matrix.

- The Al_2O_3 phase, which is only weakly bound to the AA5154 matrix, led to higher densities in samples cryomilled for 15 minutes before being sintered than those cryomilled for 30 minutes.

- Wear resistance increased from 1.2 in the AA5154-6ZrC-15 sample to 4.69 in the AA5154-18ZrC-30 sample due to the inclusion of ZrC and Al_2O_3 particles, which acted as barriers and slowed the speed. In addition to its high tensile strength, the AA5154-18ZrC-30 composite exhibited a modest elongation of 2.3% and a maximum fracture strength of around 186MPa.

- The elastic modulus and hardness range of the AA5154 matrix and ZrC composites were calculated for each composite, considering the impacts of varying cryomilling times and ZrC concentrations. Itis an excellent option because it eliminates the need to consider a transitional phase when determining the composites' hardness ratings. Both actual and theoretical hardness levels were significantly higher in aluminium alloy matrix composites supplemented with other particles than in monolithic aluminium alloy.

- Cryomilling AA5154-ZrC composites for 15 minutes and adding 18% ZrC particles showed to be more effective than either of these variables alone or in combination. Matrix-reinforcement material in AA5154-ZrC composites is entirely devoid of interference after being milled in a cryogenic environment and exposed to pressureless sintering.

References

[1] S. Khoshsima, S. Mertdinç, A. Motallebzadeh, Z. Altıntaş, D. Ağaoğulları, and Ö. Balcı-Çağıran, “Enhanced hardness and wear resistance of Al-based hybrid MMCs by using of composite metal boride reinforcement particles,” *Mater. Chem. Phys.*, vol. 288, 2022, doi: 10.1016/j.matchemphys.2022.126377.

[2] R. Das, M. K. Mondal, and S. Pramanik, “Strengthening Behaviour and Microstructural Properties during the Compaction of Reduced Blast Furnace Flue Dust—Fly Ash—Iron Metal Matrix Composite Fines using Powder Metallurgy Route,” *Trans. Indian Inst. Met.*, vol. 75, no. 9, pp. 2255–2263, 2022, doi: 10.1007/s12666-022-02592-8.

[3] V. S. S. Venkatesh and A. B. Deoghare, “Effect of microwave sintering on the mechanical characteristics of Al/kaoline/SiC hybrid composite fabricated through powder metallurgy techniques,” *Mater. Chem. Phys.*, vol. 287, 2022, doi: 10.1016/j.matchemphys.2022.126276.

[4] V. S. S. Venkatesh and A. B. Deoghare, “Effect of Sintering Mechanisms on the Mechanical Behaviour of SiC and Kaoline Reinforced Hybrid Aluminium Metal Matrix Composite Fabricated through Powder Metallurgy

Technique," *Silicon*, vol. 14, no. 10, pp. 5481–5493, 2022, doi: 10.1007/s12633-021-01333-8.

[5] E. Tekoğlu, D. Ağaoğulları, S. Mertdinç, and M. Lütfi Öveçoğlu, "Effects of reinforcement content and sequential milling on the microstructural and mechanical properties of TiB2 particulate-reinforced eutectic Al-12.6 wt% Si composites," *J. Mater. Sci.*, vol. 53, no. 4, pp. 2537–2552, 2018, doi: 10.1007/s10853-017-1687-0.

[6] M. Vijayakumar, P. Navaneethakrishnan, and G. Kumaresan, "Thermal characteristics studies on sintered wick heat pipe using CuO and Al2O3 nanofluids," *Exp. Therm. Fluid Sci.*, vol. 79, pp. 25–35, 2016.

[7] M. Li *et al.*, "Synthesis and mechanical behavior of nanostructured Al 5083/n-TiB2 metal matrix composites," *Mater. Sci. Eng. A*, vol. 656, pp. 241–248, 2016, doi: 10.1016/j.msea.2016.01.031.

[8] S. Chintada, S. P. Dora, and D. Kare, "AN OVERVIEW ON THE MICROSTRUCTURE AND MECHANICAL PROPERTIES OF SINTERED ALUMINUM-BASED COMPOSITES," *Metall. Mater. Eng.*, vol. 28, no. 1, pp. 1–16, 2022, doi: 10.30544/687.

[9] Y. Liu, X.-H. Tang, S.-F. Zhou, B.-S. Guo, Z.-G. Zhang, and W. Li, "Improving mechanical properties of Cu/Ti3AlC2 composites via in-situ decomposed gradient interfaces," *Mater. Sci. Eng. A*, vol. 834, 2022, doi: 10.1016/j.msea.2022.142615.

[10] G. Manohar, K. M. Pandey, and S. R. Maity, "Effect of sintering mechanisms on mechanical properties of AA7075/B4C composite fabricated by powder metallurgy techniques," *Ceram. Int.*, vol. 47, no. 11, pp. 15147–15154, 2021, doi: 10.1016/j.ceramint.2021.02.073.

[11] C. Lei, Y. Du, M. Zhu, W. Huo, H. Wu, and Y. Zhang, "Microstructure and mechanical properties of in situ TiC/Ti composites with a laminated structure synthesized by spark plasma sintering," *Mater. Sci. Eng. A*, vol. 812, 2021, doi: 10.1016/j.msea.2021.141136.

[12] S. Chintada, S. P. Dora, D. Kare, and P. R. V Doddi, "Developments in sintered aluminium based composites," *Met. Powder Rep.*, 2021, doi: 10.1016/j.mprp.2021.06.085.

[13] A. L. Rominiyi *et al.*, "Spark plasma sintering of Ti–Ni–TiCN composites: Microstructural characterization, densification and mechanical properties," *J. Alloys Compd.*, vol. 848, 2020, doi: 10.1016/j.jallcom.2020.156559.

[14] E. Chusong, P. Kansuwan, N. Ohtake, P. Wila, N. Tosangthum, and R. Tongsri, "Dry-sliding wear of the 316L/h-BN composites produced under crack ammonia atmosphere," *J. Met. Mater. Miner.*, vol. 30, no. 2, pp. 117–123, 2020, doi: 10.14456/jmmm.2020.28.

[15] N. Somani, Y. K. Gautam, S. K. Sharma, and M. Kumar, "Stastical analysis of dry sliding wear and friction behavior of Cu/SiC sintered composite," in *AIP Conference Proceedings*, 2018, vol. 2018. doi: 10.1063/1.5058255.

[16] M. P. Reddy, F. Ubaid, R. A. Shakoor, and A. M. A. Mohamed, "Microstructure and Mechanical Behavior of Microwave Sintered Cu50Ti50 Amorphous Alloy Reinforced Al Metal Matrix Composites," *JOM*, vol. 70, no. 6, pp. 817–822, 2018, doi: 10.1007/s11837-018-2831-2.

[17] L.-Z. Wang, Y. Liu, J.-J. Wu, and X. Zhang, "Mechanical properties and friction behaviors of CNT/AlSi10Mg composites produced by spark plasma sintering," *Int. J. Miner. Metall. Mater.*, vol. 24, no. 5, pp. 584–593, 2017, doi: 10.1007/s12613-017-1440-3.

[18] M. Tabandeh-Khorshid, J. B. Ferguson, B. F. Schultz, C.-S. Kim, K. Cho, and P. K. Rohatgi, "Strengthening mechanisms of graphene- and Al2O3-reinforced aluminum

nanocomposites synthesized by room temperature milling," *Mater. Des.*, vol. 92, pp. 79–87, 2016, doi: 10.1016/j.matdes.2015.12.007.

[19] M. Vijayakumar, S. Sivankalai, P. Michael Joseph Stalin, G. Kumaresan, P. Selvakumar, and V. Manikandan, "A scientometric Analysis on Development of Nanofluids for Heat Transfer and Fluid Flow Applications," *Solid State Technol.*, vol. 64, no. 2, pp. 3667–3684, 2021.

[20] G. Manohar, K. M. Pandey, and S. R. Maity, "Effect of microwave sintering on the microstructure and mechanical properties of AA7075/B4C/ZrC hybrid nano composite fabricated by powder metallurgy techniques," *Ceram. Int.*, vol. 47, no. 23, pp. 32610–32618, 2021, doi: 10.1016/j.ceramint.2021.08.156.

[21] G. Manohar, S. R. Maity, and K. M. Pandey, "Microstructural and Mechanical Properties of Microwave Sintered AA7075/Graphite/SiC Hybrid Composite Fabricated by Powder Metallurgy Techniques," *Silicon*, vol. 14, no. 10, pp. 5179–5189, 2022, doi: 10.1007/s12633-021-01299-7.

[22] M. Vijayakumar, P. Navaneethakrishnan, G. Kumaresan, and R. Kamatchi, "A study on heat transfer characteristics of inclined copper sintered wick heat pipe using surfactant free CuO and Al2O3 nanofluids," *J. Taiwan Inst. Chem. Eng.*, vol. 81, pp. 190–198, 2017.

[23] Z. Zhou *et al.*, "Microstructure and Ablation Behavior of W/ZrC/SiC Coating on C/C Composites Prepared by Reactive Melt Infiltration and Atmospheric Plasma Spraying," *Adv. Eng. Mater.*, vol. 23, no. 6, 2021, doi: 10.1002/adem.202001457.

[24] P. M. Kumar *et al.*, "Investigating performance of solar photovoltaic using a nano phase change material," *Mater. Today Proc.*, vol. 47, pp. 5029–5033, 2021.

[25] L. Kumar, S. Nasimul Alam, and S. K. Sahoo, "Mechanical properties, wear behavior and crystallographic texture of Al-multiwalled carbon nanotube composites developed by powder metallurgy route," *J. Compos. Mater.*, vol. 51, no. 8, pp. 1099–1117, 2017, doi: 10.1177/0021998316658946.

[26] S. Chung, B. Lee, S. Y. Lee, C. Do, and H. J. Ryu, "The effects of Y pre-alloying on the in-situ dispersoids of ODS CoCrFeMnNi high-entropy alloy," *J. Mater. Sci. Technol.*, vol. 85, pp. 62–75, 2021, doi: 10.1016/j.jmst.2020.11.081.

[27] D. Mondal, A. Zaharia, K. Mequanint, and A. S. Rizkalla, "Sol-gel derived tertiary bioactive glass–ceramic nanorods prepared via hydrothermal process and their composites with poly(Vinylpyrrolidone-Co-Vinylsilane)," *J. Funct. Biomater.*, vol. 11, no. 2, 2020, doi: 10.3390/jfb11020035.

[28] W. Grymonpré, W. De Jaeghere, E. Peeters, P. Adriaensens, J. P. Remon, and C. Vervaet, "The impact of hot-melt extrusion on the tableting behaviour of polyvinyl alcohol," *Int. J. Pharm.*, vol. 498, no. 1–2, pp. 254–262, 2016, doi: 10.1016/j.ijpharm.2015.12.020.

[29] H. S. Abdo and A. H. Seikh, "Correlation of Microstructure with Compression Behaviour of Al5083/ZrC Nanocomposites Fabricated Through Spark Plasma Sintering," *Trans. Indian Inst. Met.*, vol. 75, no. 9, pp. 2273–2280, 2022, doi: 10.1007/s12666-022-02594-6.

[30] M. Lütfi Öveçoğlu, E. Tekoğlu, S. Mertdinç, and D. Ağaoğulları, "Characterization investigations of a Al-5 wt.% Si/2 wt% (NbB2, NbC) hybrid composite fabricated via mechanically alloying and sequentially milling (mechanical alloying + cryomilling)," *Key Engineering Materials*, vol. 759 KEM. pp. 35–39, 2018. doi: 10.4028/www.scientific.net/KEM.759.35.

[31] M. Nicoara, A. Raduta, R. Parthiban, C. Locovei, J. Eckert, and M. Stoica, "Low Young's modulus Ti-based porous bulk

glassy alloy without cytotoxic elements," *Acta Biomater.*, vol. 36, pp. 323–331, 2016, doi: 10.1016/j.actbio.2016.03.020.

[32] Y.-Q. Qin *et al.*, "Enhanced mechanical and electrical properties of CuCrZr-WC alloy prepared by mechanical alloying and spark plasma sintering," *Fusion Eng. Des.*, vol. 180, 2022, doi: 10.1016/j.fusengdes.2022.113166.

[33] B. Cui *et al.*, "Microstructure and mechanical properties of vacuum brazed diamond abrasive segments with zirconium carbide reinforced Cu-based active filler metals," *Diam. Relat. Mater.*, vol. 126, 2022, doi: 10.1016/j.diamond.2022.109091.

[34] S. Jafari, M. Bavand-Vandchali, M. Mashhadi, and A. Nemati, "Synthesis mechanism and microstructure characterization of ZrB2–ZrC–SiC nanocomposite synthesized via magnesium boro/carbothermal reduction at low temperatures," *Mater. Chem. Phys.*, vol. 280, 2022, doi: 10.1016/j.matchemphys.2022.125830.

[35] R. Malkiya Rasalin Prince *et al.*, "Rapid Preparation of Al7075–B4C–ZrC Composites by Conventional Stir Casting Process: Microstructure and Tribological Studies," *Lecture Notes in Mechanical Engineering*. pp. 347–357, 2022. doi: 10.1007/978-981-19-0244-4_34.

[36] X. Kai *et al.*, "Effects of Zr element on the microstructure and mechanical properties of B4C/Al composites fabricated by melt stirring method," *Compos. Part B Eng.*, vol. 224, 2021, doi: 10.1016/j.compositesb.2021.109156.

[37] H. Li *et al.*, "Fabrication of the ZrC reinforced Ni–W composite coating and exploration of its mechanical properties and corrosion resistance," *Surf. Coatings Technol.*, vol. 421, 2021, doi: 10.1016/j.surfcoat.2021.127413.

[38] Z. Zhao *et al.*, "Microstructure and mechanical properties of ZrC coating on zirconium fabricated by interstitial carburization," *J. Alloys Compd.*, vol. 834, 2020, doi: 10.1016/j.jallcom.2020.155110.

[39] C. Lv, X. Ren, C. Wang, and Z. Peng, "Spark plasma sintering of ultrafine WC-10Ni-ZrC hardmetals: Effects of adding ZrC nano-powder," *Int. J. Appl. Ceram. Technol.*, vol. 17, no. 3, pp. 932–940, 2020, doi: 10.1111/ijac.13475.

[40] D. Liu, T. Yang, H. Ma, and Y. Liang, "The microstructure, bio-tribological properties, and biocompatibility of titanium surfaces with graded zirconium incorporation in amorphous carbon bioceramic composite films," *Surf. Coatings Technol.*, vol. 385, 2020, doi: 10.1016/j.surfcoat.2020.125391.

[41] C. Zeng *et al.*, "The effect of sol-gel process on the microstructure and particle size of ZrC–SiC composite powders," *Ceram. Int.*, vol. 46, no. 4, pp. 5244–5251, 2020, doi: 10.1016/j.ceramint.2019.10.273.

[42] P. Samal, B. Surekha, and P. R. Vundavilli, "Experimental Investigations on Microstructure, Mechanical Behavior and Tribological analysis of AA5154/SiC Composites by Stir Casting," *Silicon*, vol. 14, no. 7, pp. 3317–3328, 2022, doi: 10.1007/s12633-021-01115-2.

[43] A. Zykova *et al.*, "Microstructural Evolution of AA5154 Layers Intermixed with Mo Powder during Electron Beam Wire-Feed Additive Manufacturing (EBAM)," *Metals (Basel).*, vol. 12, no. 1, 2022, doi: 10.3390/met12010109.

[44] C. Wu *et al.*, "Influence of coarse grain particles on mechanical properties and fracture behavior in multi-modal Al-based metal matrix composites," *Powder Technol.*, vol. 394, pp. 901–908, 2021, doi: 10.1016/j.powtec.2021.09.027.

[45] S. Saimoto, P. Van Houtte, K. Inal, and M. R. Langille, "New biaxial yield function for aluminum alloys based on plastic work and work-hardening analyses," *Acta Mater.*, vol.

118, pp. 109–119, 2016, doi: 10.1016/j.actamat.2016.07.036.

[46] E. Tekoğlu, Y. Yürektürk, D. Ağaoğullarl, S. A. A. Dilawary, M. Baydoğan, and M. L. Öveçoğlu, "Investigation of indentation and dry sliding wear behaviour of Al-12.6 wt.% Si-10 wt.% TiB2composites produced by sequential milling and pressureless sintering," *Int. J. Mater. Res.*, vol. 110, no. 11, pp. 1047–1057, 2019, doi: 10.3139/146.111830.

[47] C. Wu *et al.*, "Interfacial segregation and precipitates behavior in the ultrafine grained Al-based metal matrix composites," *J. Alloys Compd.*, vol. 770, pp. 625–630, 2019, doi: 10.1016/j.jallcom.2018.08.183.

[48] Ö. Balcı, D. Ağaoğulları, H. Gökçe, M. L. Öveçoğlu, and M. Somer, "Effect of cryomilling on matrix/reinforcement interfaces and properties of Al-TiB2 composites," *J. Alloys Compd.*, vol. 757, pp. 393–402, 2018, doi: 10.1016/j.jallcom.2018.05.098.

[49] S. Mertdinç, E. Tekoğlu, D. Ağaoğullari, and M. L. Öveçoğlu, "Influence of the milling process on TiB2 particle reinforced Al-7 wt.-% Si matrix composites," *Mater. Test.*, vol. 60, no. 7–8, pp. 719–726, 2018, doi: 10.3139/120.111207.

[50] X. Cai *et al.*, "Thermally stable and strong bulk Mg–MgO in situ nanocomposites by reactive cryomilling and high-pressure consolidation," *J. Mater. Sci.*, vol. 53, no. 9, pp. 6613–6625, 2018, doi: 10.1007/s10853-018-2041-x.

[51] R. Cohn, B. Fullenwider, K. Ma, and J. M. Schoenung, "Calorimetric study with uncertainty analysis to investigate the precipitation kinetics in a nanostructured Al composite," *Adv. Eng. Mater.*, vol. 20, no. 4, 2018, doi: 10.1002/adem.201700728.